Polyindene/Organo-Montmorillonite Conducting Nanocomposites. II. Electrorheological Properties

Serkan Guzel, Ozlem Erol, H. Ibrahim Unal

Chemistry Department, Gazi University, Smart Materials Research Laboratory, Teknikokullar, Ankara, Turkey

Received 24 January 2011; accepted 5 September 2011
DOI 10.1002/app.35594
Published online 11 December 2011 in Wiley Online Library (wileyonlinelibrary.com).

ABSTRACT: In this study, polyindene (PIn) and three PIn/organo-montmorillonite (O-MMT) nanocomposites namely K1: [PIn(94.5%)/O-MMT(5.5%)], K2: [PIn(92.8%)/O-MMT(7.2%)], and K3: [PIn(87.9%)/O-MMT(12.1%)] were used to investigate the electrorheological (ER), creep-recovery, and vibration damping characteristics. A volume fraction series (φ = 5–25%) of suspensions were prepared from the samples in silicone oil (SO). First, zeta (ζ)-potentials and antisedimentation stabilities; second, ER properties of these nanocomposite/SO suspension systems were determined under externally applied electric field strengths. Besides, the effects of dispersed phase volume fraction, shear rate, electric field strength, and temperature onto ER performance of these suspensions were investigated and non-Newtonian rheological behaviors were observed. The vibration damping capabilities of the suspensions were investigated using various rheological parameters on the electrorheometer and on an automobile shock absorber and a 66% vibration damping capacity were determined under an applied electric field strength, which is an important property from industrial point of view. Furthermore, the materials were subjected to creep and creep-recovery tests and reversible viscoelastic deformations were determined. From the experiments carried out, the nanocomposites were classified as smart materials. © 2011 Wiley Periodicals, Inc. J Appl Polym Sci 124: 4935–4944, 2012

Key words: polyindene; montmorillonite; polymer–matrix composites; electrorheological properties; creep-recovery; vibration damping

INTRODUCTION

Smart materials, whose properties change with an external stimulus such as temperature, electric field, magnetic field, or chemicals, have significant features of useful effects which can be easily controlled with changing the environmental conditions. Electrorheological (ER) fluids are classified as smart materials. Their rheological properties under adequate external electric fields are impressively changed within a millisecond and in a reversible manner. They can switch from a liquid-like material to a solid-like under the application of an external electric field and this phenomenon is called the ER effect. Because of their controllable viscosity and short response time, ER fluids can therefore be used as electrical and mechanical interfaces in various industries such as automotive, robotics, brakes, clutches, shock absorbers, actuators, and active devices.[1] However, the commercializations of these applications are still restricted because of some unsolved problems, such as poor temperature and low antisedimentation stability, abrasion, and the requirement of higher yield stresses at low electric field strengths.[2]

ER fluids are composed of a suspension of micron-sized semiconducting or conducting polarizable particles in an insulating non-polar liquid such as mineral, paraffine, or silicone oils (SOs). ER effect is controlled by a number of parameters, including the volume fractions, the electrical conductivities, permittivities, sizes, and shapes of the of dispersed phase particles; and the contents of any promoter and other additives in the dispersed and continuous phases.[3,4]

Conducting polymers are popularly used as ER materials, since they can easily be prepared with a controllable conductivity. Some conductive polymers such as polyaniline and polypyrrole are soft and non-abrasive materials to be used for ER device applications, and have attracted a great deal of attention over the past few years, reported in a large number of technical publications.[5] However, several problems are associated with these systems such as poor dispersion stability due to the strong particle aggregation and high current density. Various approaches have thus been proposed to modify the surfaces of these conducting polymers with various methods to improve their ER performance. Many ER

Correspondence to: H. I. Unal (hiunal@gazi.edu.tr).
Contract grant sponsor: Turkish Scientific and Technological Research Council; contract grant number: 107 T 711.
Contract grant sponsor: European Science Foundation (COST Action D43).

materials based on polymer/inorganic composites or nanocomposites are expected to have the advantages of both polymeric and inorganic ER materials.[6]

Montmorillonite (MMT) clay has been widely used for preparing polymer/clay nanocomposites to improve their engineering applicability with better dispersion stability, mechanical strength, or physical properties. Its unique crystal structure exhibits octahedral aluminate sheets sandwiched between tetrahedral silicate layers, where water or organic molecules are introduced between the layers and the layer charge can easily be controlled by exchange of cations in the galleries of MMT layers with different charges. The mobility of metal cations is found to play a critical role in the ER response of these systems. The aluminosilicate materials are very attractive due to their strong ER performance. Since the ER effect is associated with the mobility of metal cations in this type of materials, the current density is relatively high, contributed to the movement of metal cations, adsorbed moisture, or crystallized water especially at high temperatures. Another shortcoming is the particle sedimentation, which can be partially overcomed using suitable surfactants or preparing hybrid nanocomposites.[1]

Conducting polymer/clay nanocomposites including polyaniline[7] and polypyrrole[8] have large attentions from the ER community due to their enhanced ER characteristics. Also, researches are being carried out to find out the best colloidally stable and high performance ER fluids.

In this study, polyindene (PIn) and *in-situ* polymerized PIn/organo-montmorillonite (O-MMT) nanocomposites were used as ER active materials. To overcome the problems arising from the mobility of metal cations, crude bentonite was enriched in Na-MMT to obtain better intercalation properties in the final product of nanocomposite, when compared with the Ca-MMT.[9] Their ζ-potentials in non-aqueous medium were determined. Then, a series of suspensions were prepared in SO to investigate their ER activities. In this manner, after determining the anti-sedimentation stabilities, the effects of dispersed particle volume fraction, electric field strength, shear rate, temperature, and frequency onto ER performance of the materials were investigated, creep-recovery characteristics were examined and vibration damping capabilities were determined.

EXPERIMENTAL

Materials

SO was provided from Aldrich ($\rho = 0.965$ g cm^{-3}, $\eta = 1$ Pa s, $\varepsilon = 2.61$ at 25°C). Natural bentonite was kindly supplied by Samas Co of Istanbul; enriched to increase the content of Na-MMT and then organically modified with cetyltrimethylammonium bromide [CTAB, $C_{16}H_{33}N(CH_3)_3{}^+Br^-$] to obtain organically modified O-MMT.

Synthesis of PIn and PIn/O-MMT nanocomposites

PIn and PIn/O-MMT nanocomposites were *in-situ* polymerized using $FeCl_3$ as an oxidizing agent in CH_3Cl at 15–20°C for overnight taking the ratio of monomer to oxidant as 1 : 1. Then the crude products were washed with deionized water and diethylether, respectively and vacuum dried before use. They were charterized by Fourier transform infrared, X-ray diffraction, thermogravimetric analysis, scanning electron microscopy, conductivity, dielectric, density, and particle size measurements. Details of the synthesis and full characterization of PIn and PIn/O-MMT nanocomposites are given in our previous publication.[10]

Preparation of suspensions

Known amounts of vacuum dried Na-MMT, O-MMT, PIn, and PIn/O-MMT particles were dispersed in SO and suspensions were prepared at a series of volume fractions ($\varphi = 5$–25%), by dispersing definite amount of dispersed phase in calculated amount of continuous phase (SO) according to the formula:

$$\varphi = \left[\frac{V_{\text{dispersed particles}}}{V_{\text{dispersed particles}} + V_{\text{SO}}}\right] \times 100 \qquad (1)$$

Antisedimentation ratio measurements

Determination of the anti-sedimentation ratios which are defined to be proportional to the stability against gravitational forces of the suspension systems were measured as following: glass tubes containing various volume fractions of the above suspensions were immersed into a constant temperature ($T = 25 \pm 0.1$°C) water bath. During the neat eye observations, the height of phase separation between the particle-rich phase and the relatively clear oil-rich phase was recorded as a function of time by using a digital composing stick. The anti-sedimentation ratio (%) was defined as the height of the particle-rich phase divided to the total height of suspension as schematically inserted in to Figure 1.

Zeta potential measurements

Zeta(ζ)-potentials of the colloidal dispersions were measured by a Malvern Nano-ZS zeta potential analyzer which works with Laser Doppler

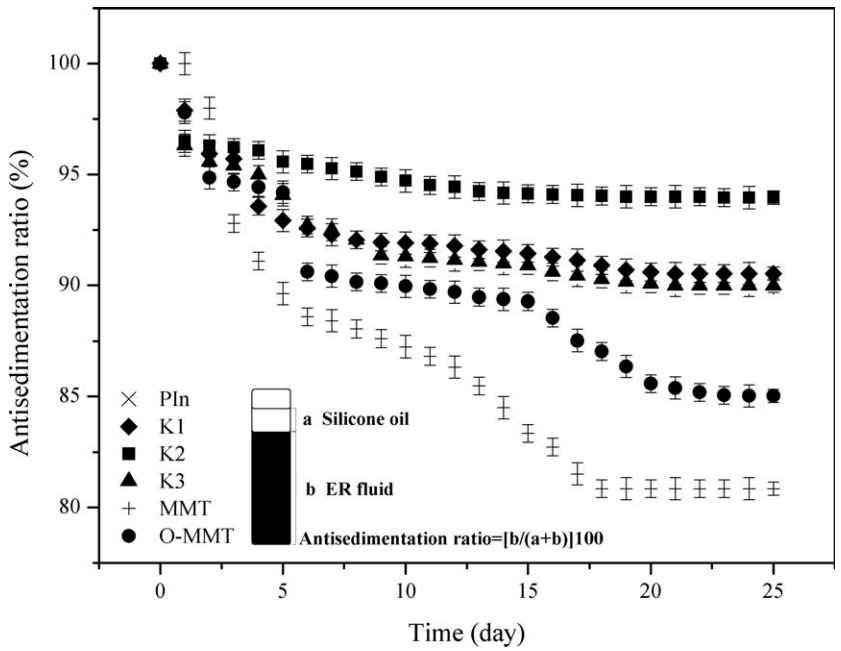

Figure 1 Antisedimentation stability results of the suspensions ($\varphi = 25\%$, $T = 25°C$).

Electrophoresis technique by using phase analysis light scattering. The self optimization routine (laser attenuation and data collection time) in the Zeta-Sizer software was used for all the measurements. The ζ-potentials of the materials colloidally dispersed in SO ($\eta = 4.57 \times 10^{-3}$ Pa s, Aldrich), having the concentration of 1×10^{-2} g/L, were measured using a dip-cell and calculated according to the Hückel approximation.

Flow measurements

Flow rate measurements were carried out between two brass electrodes, which were connected to a high-voltage dc power supply (see inset in Fig. 3). The gap between the electrodes was 0.5 cm, the width of the electrodes was 1.0 cm, and the height of the suspensions on the electrodes was 5.0 cm. Before each measurement to be carried out, suspensions were mechanically stirred against sedimentation. During the measurements, the electrodes was immersed into a vessel containing the suspensions, with a specific volume fraction, and after a few seconds, the vessel was removed and the flow time for complete drainage measured, using a digital stopwatch under $E = 0$ kV/mm and $E \neq 0$ kV/mm conditions. This procedure was repeated for various E values and volume fractions of the suspensions.

Electrorheogical measurements

ER properties of the suspensions were determined with a Termo-Haake RS600 parallel plate torque electro-rheometer. The gap between the parallel plates was 1.0 mm and the diameters of the upper and lower plates were 35 mm. The potential used in these experiments was supplied by a 0–12.5 kV (with 0.5 kV increments) dc electric field generator (Fug Electronics, HCL 14, Germany), which enabled resistivity to be created during the experiments.

Vibration damping experiments on an automobile shock absorber

Since approximately 250 mL of suspension was needed for this real time vibration damping experiment carried out on a modified Skoda automobile shock absorber, Na-MMT was used as a dispersed phase in SO at a volume fraction of 10%, and the vibrations recorded by Therpa Hydraulic vibration damping test equipment under $E = 0$–250 V/mm conditions at the Automotive Engineering Department. The hydraulic vibration test equipment contained a wheel (with a spring coefficient of 65,400 N/m), an axle, a spring (with a coefficient of 13,000 N/m), a shock absorber, an electrically operated drum to turn the wheel, a vibrating mass (60 kg), a non-vibrating mass (14 kg), control units, and an external electric field generator (Fug electronic). During the experiments, vibrations occurring on the body and on the axle were recorded by a recorder which was operated at 400 V and 16 Amps.

Creep and creep-recovery measurements

During the creep and creep-recovery experiments, a constant stress ($\tau_o = 5$ Pa) was applied instantaneously ($t = 10$ s) to PIn/SO, K1/SO, K2/SO, and K3/

TABLE I
Some Physical Characteristics of the Samples

Sample	Conductivity[a] (σ, S cm^{-1})	Dielectric constant[a]	Density[a] (ρ, g cm^{-3})	Average particle size[a] ($d_{0.5}$, μm)	Recoverable strain, % (E = 2 kV/mm)
PIn	9.3×10^{-6}	4.3	1.04	1.1	87
Na-MMT	5.9×10^{-7}	7.5	1.88	9.2	–
O-MMT	2.8×10^{-7}	6.5	1.58	5.5	–
K1	5.5×10^{-6}	4.1	1.07	2.2	86
K2	5.1×10^{-6}	5.8	1.08	2.3	81
K3	3.7×10^{-6}	5.9	1.09	3.8	77

[a] See Ref. 7.

SO suspension systems and changes in strains (γ) were measured over a period of time. Then the stress was set to $\tau_o = 0$ Pa and with these measurements the recoverable elastic portions of the deformations were determined.

RESULTS AND DISCUSSIONS

Antisedimentation stabilities of the suspensions

Gravitational stability is one of the most important desired parameter, which determines the suspension's industrial applicability for ER fluids. They are expected to be stable against gravitational forces for a long time in hard environmental conditions and not to leave deposite. It is known that ER activity is formed because of chain formation perpendicular to the direction of electric field via electric field induced attractive forces between the dispersed particles. There are various parameters which affect the gravitational stability and long term ER activity of a suspension, namely (i) sizes of the dispersed particles, (ii) type of the dispersed particles (*i.e.*, hollow, porous, lamellar), (iii) type, viscosity, and density of the dispersion medium, (iv) humidity of the environment, (v) presence of the surfactants.

To meet these requirements, in this study, the materials were subjected to ground milling to obtain possible smallest particle size of the dispersed materials. Then, to investigate the effect of type of the dispersed phase, a series of dispersions were prepared from Na-MMT, O-MMT, PIn, K1, K2, and K3 nanocomposites in SO dispersion medium at a volume fraction of 25%, and results obtained are depicted in Figure 1. Antisedimentation ratio (unsettled portion of the dispersion) of MMT was observed to be the smallest one due to the flake-like structure which makes easier the particles to coagulate. Antisedimentation ratio of O-MMT was higher than Na-MMT which may be attributed to the presence of surfactant CTAB in the layers and on the surfaces of O-MMT lamellar structure.

According to Figure 1, PIn showed the highest antisedimentation ratio as expected. The PIn/O-MMT nanocomposite suspensions possessed an excellent anti-sedimentation stability and were observed to increase with increasing PIn content, due to the raised intercalation fraction of PIn into MMT galleries, which is supported with the changes in their apparent densities and particle size distributions (See Table I). The suspension systems observed to show fast reduction of sedimentation and reached to metastable equilibria resulting with intermediate plateaus and then restarted to agglomerate, before reaching to the steady-state. As a consequence, the PIn/O-MMT nanocomposites can be dispersed into SO very well for ER measurements and do not deposite even when they are static for more than 25 days and reach to the steady state.

Since K2/SO suspension showed the highest antisedimentation stability, the effect of volume fraction on the anti-sedimentation ratios was investigated only for this system. The results obtained after the system reached to the steady state at the end of 25 days are as following: $(95\%)_{\varphi=25\%} > (94\%)_{\varphi=20} > (92\%)_{\varphi=15\%} > (88\%)_{\varphi=10\%} > (75\%)_{\varphi=5\%}$. It was concluded that, in this system, at the lower volume fractions the gravitational forces, which reduces the colloidal stability of suspension, and at the higher volume fractions the repulsive electrostatic forces, which increase the colloidal stability of suspensions, are dominant between the increased numbers of dispersed particles. The 95% sedimentation ratio is a perfect result for PIn/O-MMT nanocomposites for future potential industrial ER applications.

Sarikaya et al.[11] reported 80% antisedimentation ratio for PIn/$CaCO_3$/SO and Xiang et al.[12] reported 97% anti-sedimentation ratio for poly(N-methylaniline)/MMT-nanocomposite/SO (φ = 5%) suspension systems.

Zeta potential results in non-aqueous medium

In the presence of an electric field, it is necessary to take the electrophoretic force exerted by the field on the particles having a net charge into account, which being related with the ζ-potential of the solid phase in the suspending liquid. For ER fluids, surface charges and presence of polar groups in the

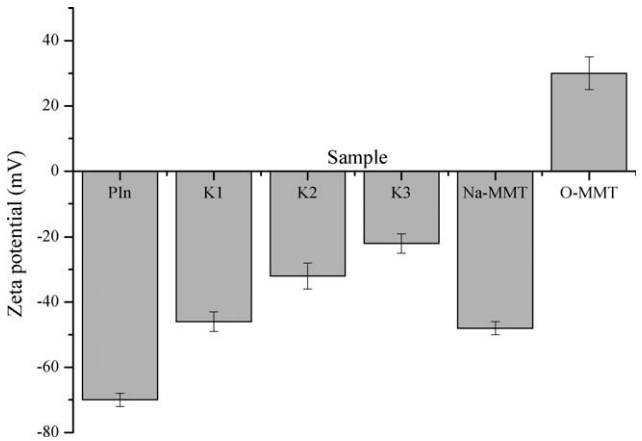

Figure 2 Zeta potentials of the materials in silicone oil ($c = 0.01$ g/L, $T = 25°C$).

structure of the dispersed particles are important. The ζ-potentials of the materials measured in SO are shown in Figure 2. The materials were shown negative ζ-potentials, except O-MMT. The positive ζ-potential of O-MMT is a result of the orientation of the cationic surfactant (CTAB, $C_{16}H_{33}N(CH_3)_3^+Br^-$) molecules on the surfaces of Na-MMT particles. On the other hand, for the PIn/O-MMT nanocomposites, ζ-potential values were negative and shifted to regions that became more negative with the increasing amount of PIn content, indicating more colloidally stable condition. This may be attributed to the dominant factor of negatively charged $[FeCl_4]^-$ ions which surround the suspended PIn particles and cause electrostatic repulsions. Also the gravitational forces generally lead to sedimentation at a rate which depends on the sizes of the dispersed particles, on the density mismatch between the liquid and solid phases and on the hydrodynamic forces. These statements are especially true for PIn/O-MMT nanocomposites, which showed ζ-potentials shifting to the region that became more negative with decreasing average hydrodynamic sizes of the dispersed particles.

Electrorheological studies

When an ER suspension is subjected to an external electric field (E), the response time and threshold energy (E_t, the first significant increment of flow time under E) of the dispersed particles are very important for industrial applications, which are desired to be milliseconds and volts reversibly and repeatedly. To observe the effect of dc electric field on the ER activity, flow rate measurements were carried out and the effects of dispersed particle type [Fig. 3(a)] and volume fraction [Fig. 3(b)] were investigated on the E_t of the materials.

When E is applied, the field induced interactions cause dispersed particles to have effective motions relative to the SO phase, which virtually end up with dramatic shear viscosity enhancement between the electrodes. As seen from Figure 3(a), threshold energies were observed to increase generally with increasing conductivity and decreasing dielectric constant (see Table I) of the dispersed materials. On the other hand, when the effect of dispersed phase volume fraction was taken into account [Fig. 3(b)], threshold energies were observed to decrease with increasing volume fraction, as a result of the dominated electric field induced polarization forces acting between the dispersed particles, and causing firstly fibrillar then stripe and finally the strongest columnar structures between the upper and lower plates of the electrorheometer, as expected. This behavior is in consistence with the most of the ER fluids and it can be concluded that the interparticle distances of the dispersed particles in the suspension decrease when the

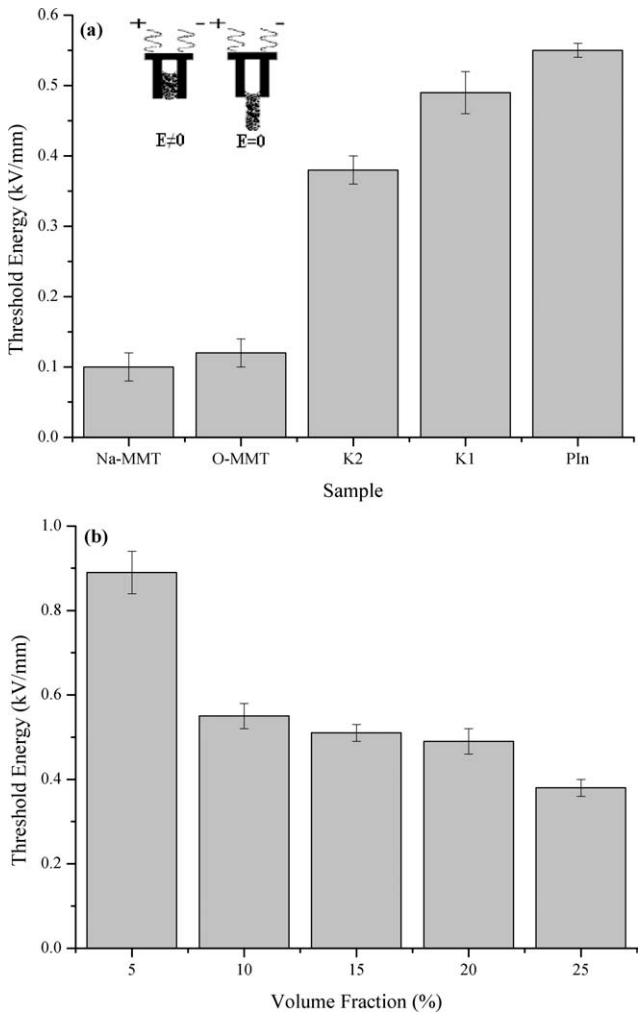

Figure 3 (a) Effect of the type of material on threshold energy (φ = 25%), (b) Effect of volume fraction on threshold energy (Sample: K2/SO).

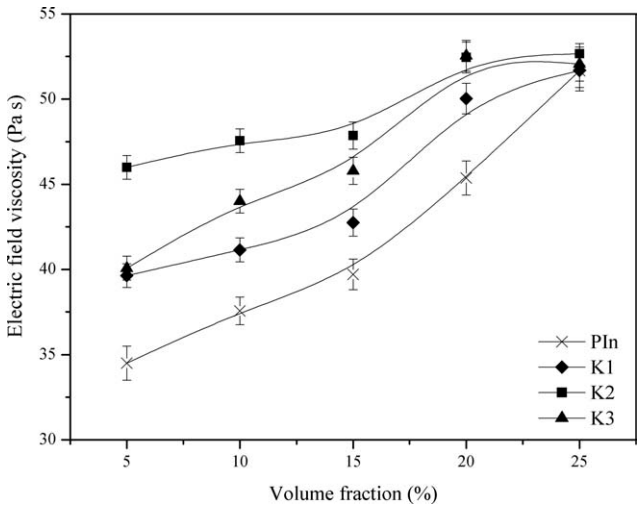

Figure 4 Effect of volume fraction on electric field viscosity ($E = 3$ kV/mm, $\dot{\gamma} = 1\ s^{-1}$, $T = 25°C$).

concentration increase and E_t tends to be lower. Response times (the time required for typical ER suspension to respond to a step increase of E) of hematite/SO suspensions under the dc fields were reported to be on a time scale of seconds to reach a steady-state after the application of E by Espin et al.[13]

Effects of volume fraction on electric field viscosity and shear stress

The magnitude of polarization forces (F_p) acting between the dispersed particles are responsible for elevated electric field induced viscosities (η_E) of the suspensions, which is given by the following equation:[14]

$$F_P = \frac{6\varepsilon_2 r^6 E^2}{h^4} \quad (2)$$

where ε_2 is the dielectric constant, r is the radius of dispersed particles and h is the distance between dispersed particles.

According to this equation, decreased h causes an increase on the magnitude of F_p which results with enhanced η_E of the suspensions. It is known that particle volume fraction significantly affects the apparent viscosity of the suspension. In the literature, linear or parabolic increases on η_E or electric field induced shear stress were reported with increasing dispersed phase volume fraction, as a result of increased F_p.[15,16] On the other hand, there could be a critical particle volume fraction for each ER fluid which causes different effects on each individual system. For this reason, to investigate the effect of dispersed phase volume fraction on η_E, a series of suspensions (φ = 5–25%) were prepared from the materials in SO at constant conditions and results obtained are depicted in Figure 4. In all the suspension systems examined, gradual increases were observed on η_E with increasing φ values due to the enhanced F_p between the dispersed particles. Nevertheless, at higher volume fractions, increments on η_E were not high enough, incontrast to the expectations, which is in accordance with the changes of dielectric constant values of the dispersed particles in SO, being very close to each other (Table I). It was reported for chitin/SO suspension system that decreased distance between the particles cause increases on the mutual actions between the dispersed particles, and as a result electrical double layers around the particles may drop out.[17]

Shear stress (τ) is a measure of fluids resistivity againts flow in ER fluids. Volume fraction of a suspension is one of the major factors that affect the value of ER suspension's shear stress. The value of τ increases with increasing φ and its ideal value depends on the purpose of application. For example, on dynamic vibration damping systems, response time and non-abrasive properties of ER suspension are more important than high values of τ.

Linear relationships were observed between φ and electric field induced shear stresses (τ_E) of materials' suspensions. For PIn/SO system $\tau_E = 6.9$ Pa was obtained at $\varphi = 5\%$ and increased to $\tau_E = 10.3$ Pa at $\varphi = 25\%$. Between the nanocomposites examined, the highest τ_E increment was determined for K2/SO system with $\Delta\tau_E = 1.7$ Pa shear stress increase when φ was increased from 5 to 25% (Fig. 5). Similarly, Choi et al. reported in their two different studies that τ_E inceased with increasing φ for cellulose phosphate ester/SO suspensions[18] but, τ_E first increased upto a critical φ and then slightly decreased for chitosan phosphate/SO system.[19]

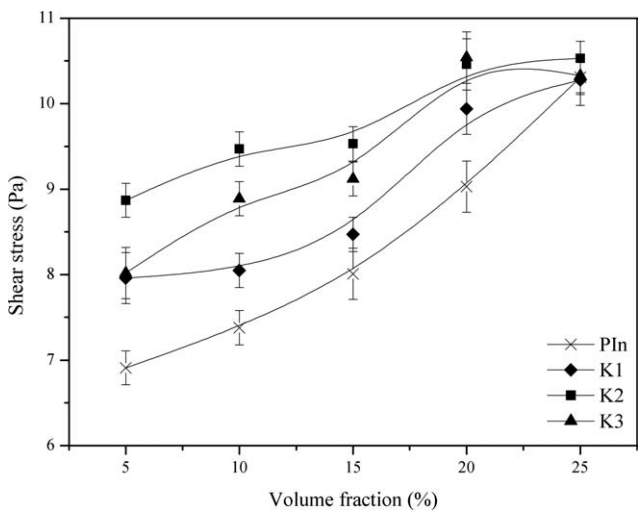

Figure 5 Effect of volume fraction on shear stress ($E = 3$ kV/mm, $\dot{\gamma} = 1\ s^{-1}$, $T = 25°C$).

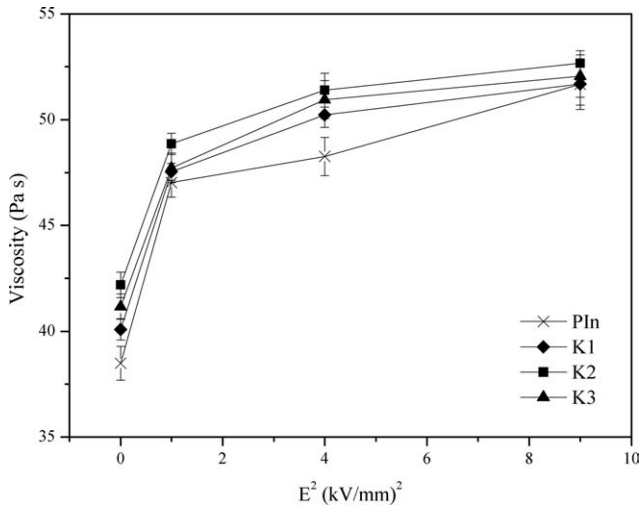

Figure 6 Effect of electric field strength square on viscosity ($\varphi = 25\%$, $\dot{\gamma} = 1\ s^{-1}$, $T = 25°C$).

Effects of electric field strength on viscosity and shear stress

A chain structure is formed between the dispersed particles in an ER fluid under the influence of external electric field strength with the influence of various parameters such as polarization forces, hydrodynamic forces at the mobile phase, Brownian motions, short range electrostatic attractive and repulsive forces, steric interactions, adhesive forces, van der Waals attractive forces, and the presence of promoters.[20] The structure and magnitude of ER response depend on the race between these forces.

Figure 6 shows the effect of E and type of material on η_E, which is studied at the optimum volume fraction of 25%. Sharp increases on the η_E were observed up to $E = 1$ kV/mm then the PIn/O-MMT/SO suspensions reached to the steady-state condition. The highest η_E was obtained for K2/SO system as 53 Pa s. Similar trend was reported in the literature for polyindole/O-MMT nanocomposite/SO system and PIn/$CaCO_3$/SO system.[9,11]

Figure 7 shows the power law dependence of τ_E to E upto $E = 1$ kV/mm in accordance with the relationship given below and then the system reached to the steady-state:

$$\tau_E \propto \varphi K_f E^2 \beta^2 \quad (3)$$

where K_f is the dielectric permittivity of dispersing medium, β is the polarizability measured at dc electric fields.[21] The highest τ_E was determined for K2/SO system under $E = 3$ kV/mm as 10.5 Pa.

Effects of shear rate on shear stress and viscosity

The effects of shear rate on shear stress and viscosity of PIn and PIn/O-MMT nanocomposites were investigated at $E = 0$ and $E = 3$ kV/mm conditions and results obtained just for K2/SO system is depicted in Figure 8, since the other samples show the same kind of behaviors. Increments were observed for all the materials examined with rising shear rates. For K2/SO system under $E = 3$ kV and $\dot{\gamma} = 100\ s^{-1}$ conditions, the change of τ_E were in the following order: $\tau_{K3} = 284$ Pa $> \tau_{K2} = 281$ Pa $> \tau_{PIn} = 255$ Pa $> \tau_{K1} = 237$ Pa. Also, yield stresses (τ_y), calculated from the shear stress–shear rate graphs obtained at control rate (CR) mode by extrapolating the flow curve to $\dot{\gamma} = 0\ s^{-1}$, are determined to be in the following order: $\tau_{y(K1)} = 8.9$ Pa $> \tau_{y(K3)} = 7.5$ Pa $> \tau_{y(K2)} = 6.8$ Pa $> \tau_{y(PIn)} = 5.6$ Pa.

Non-Newtonian shear thinning viscoelastic behaviors were observed for all the materials examined under the influence of shear rate. As seen from Figure 8, for K2/SO system, exponential viscosity decrease were observed up to $\dot{\gamma} = 10\ s^{-1}$ and then

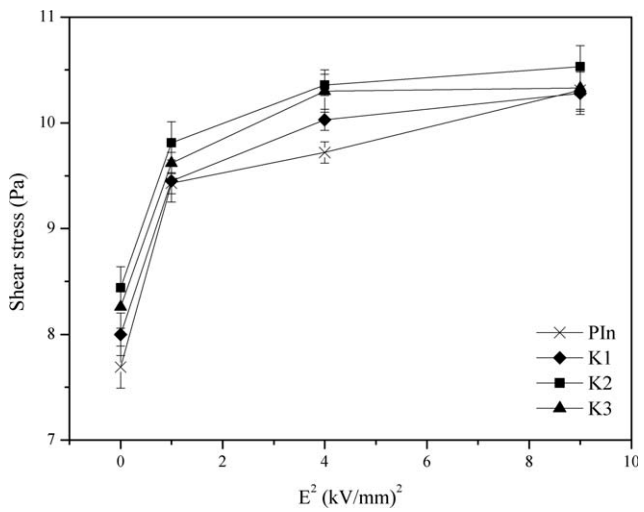

Figure 7 Effect of electric field strength square on shear stress ($\varphi = 25\%$, $\dot{\gamma} = 1\ s^{-1}$, $T = 25°C$).

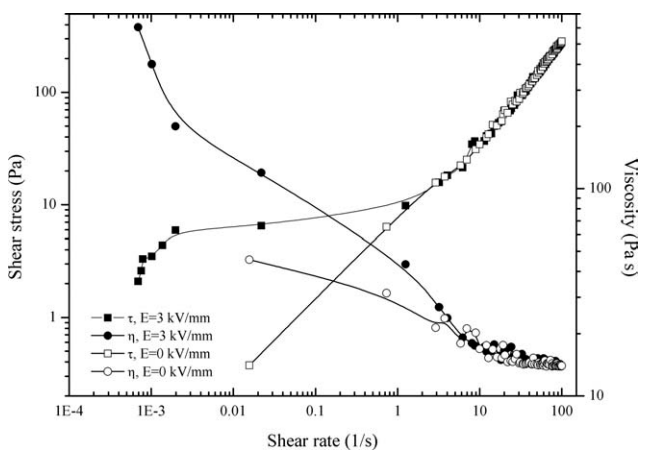

Figure 8 Effects of shear rate on shear stress and viscosity ($\varphi = 25\%$, $T = 25°C$).

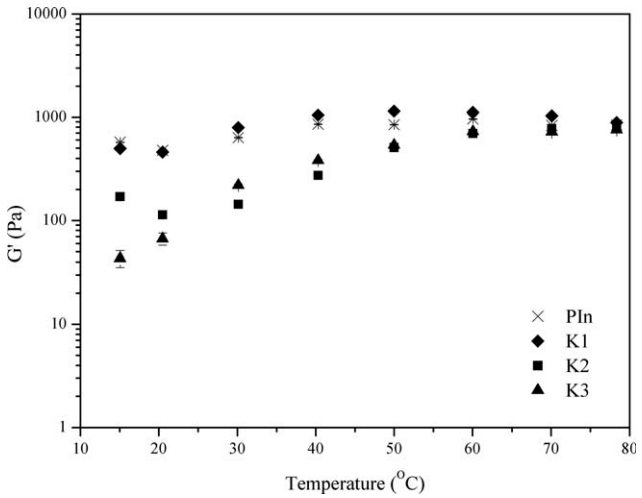

Figure 9 Effect of temperature on storage modulus (φ = 25%, E = 3 kV/mm, τ = 1 Pa, f = 1 Hz).

become shear rate independent, which indicate the collapse of ER chain formation as a result of shearing forces.

Effect of temperature on storage modulus

It is known that, several factors are associated with the temperature effect on the ER performance: (i) elevated temperature may cause ER strength losses due to the weakened polarization, decreased conductivity, increased dielectric losses, and current density, (ii) elevated temperatures increase the number of collisions between the dispersed particles by increasing particles' thermal motion. If the magnitude of this thermal motion is big enough to compete with the particle fibrillation, it may end up with a weakened ER fibrillar structure. The ultimate ER effect comes from the balance attained among the above factors.[22]

Within the temperature range studied (15–80°C) increases were determined on the storage modulus (G') values of the materials examined (Fig. 9). It was observed that the temperature positively affects the G' values of the suspensions. The fibrillar structures become more rigid or elastic with increasing temperature due to the stronger particle polarization. Also, decreased viscosity of the dispersant phase with increasing temperature may make chain formation relatively easy, and then improve the elasticity for these suspension systems.[23] It was observed that PIn and K1 (5.5% O-MMT content) showed, almost identical, slightly increasing G' behavior at elevated temperatures. K2 (7.2% O-MMT content) first showed gradual decreasing G' and after 30°C it positively responded to the raised temperatures and showed G' increments. K3 (12.1% O-MMT content) showed gradual increase on G' with increasing temperature which may be attributed to the increasing amount of O-MMT in the PIn/O-MMT nanocomposite structures.

Effect of frequency on viscoelasticity

Viscoelastic properties are one of the main parameters to be investigated to determine the vibration damping capability of the materials. The frequency sweep was carried out to describe how the ER structures manifest themselves in the viscoelasticity in the dispersions. For this purpose, a series of experiments were carried out under f = 0−100 Hz conditions for PIn and PIn/O-MMT nanocomposites and tan δ *versus* frequency graph is shown in Figure 10. As reflected from the graph, except K1 [(PIn(94.5%)/O-MMT(5.5%)], which shown elastic behavior with increasing frequency, the rest of the materials were showed viscous behavior at the beginning of the frequency sweep experiment, but PIn become to be gel like at elevated frequencies.[24]

Vibration damping experiments on an automobile shock absorber

Due to the amount of sample required (approximately 250 mL), vibration damping experiments were only carried out using Na-MMT/SO suspensions at constant conditions and results obtained from the body (a) and axle (b) are depicted in Figure 11.

Positive body vibration amplitudes (recorded in the course of opening of the shock absorber) were observed to bigger than the negative body vibration amplitudes (recorded in the course of closing of the shock absorber).[25] The magnitude of these body vibration amplitudes were a_{body} = 13.75 mm when E = 0 kV/mm (no ER effect) and reduced to a_{body} = 4.65 mm when E = 0.25 kV/mm (with ER effect). In a similar way, the axle vibration amplitudes were

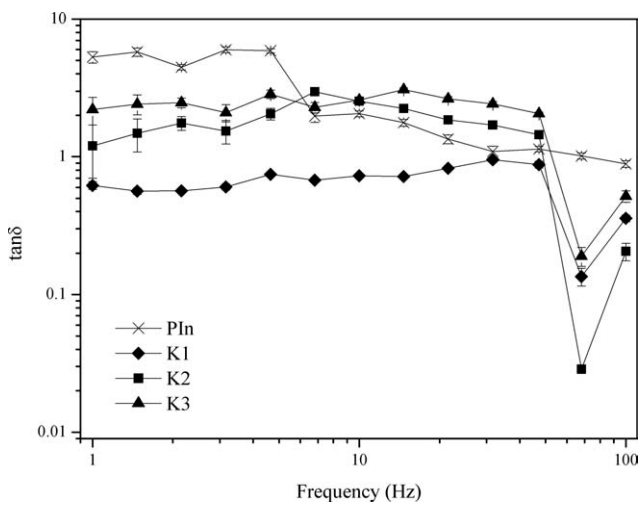

Figure 10 Change in tan δ with frequency (E = 3 kV/mm, φ = 25%, τ = 1 Pa, T = 25°C).

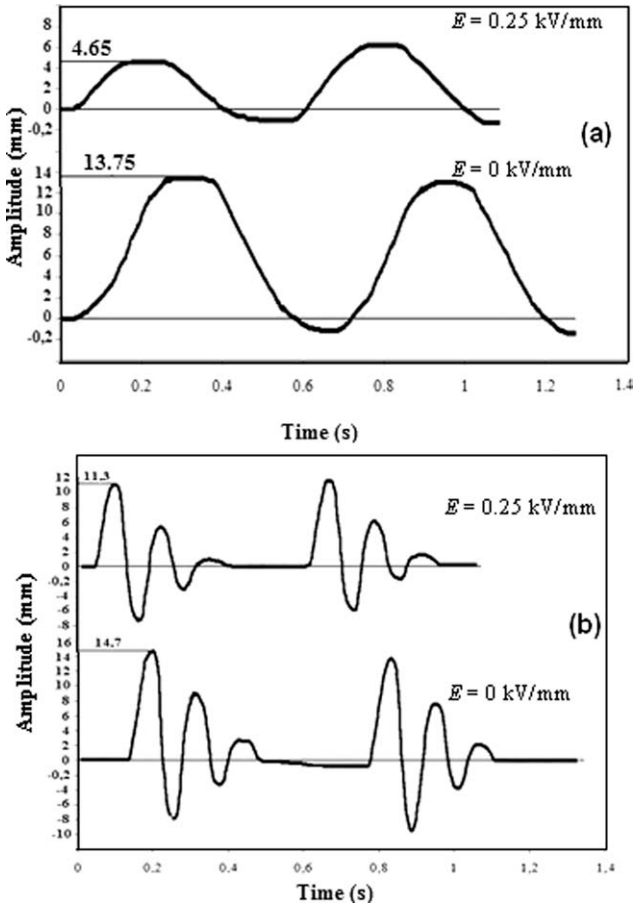

Figure 11 Vibration damping graph of the shock absorber: (a) On the body, (b) on the axle (Sample: Na-MMT/SO, φ = 10%).

determined to be $a_{axle} = 14.7$ mm when $E = 0$ kV/mm (no ER effect) and reduced to $a_{axle} = 11.3$ mm when $E = 0.25$ kV/mm (with ER effect). Thus, we obtained vibration damping values of 66% and 23% on the body and on the axle of the automobile shock absorber respectively, which are very important from potential industrial applications points of view.

Creep and creep-recovery results

Creep and creep-recovery tests are one of the critical methods to obtain information on deformation and recovery behaviors of the materials. In creep and creep-recovery tests, an instantaneous strain is applied to the material under isothermal conditions and change in strain (γ) is measured. Some deformations can be recoverable when the applied stress is removed. The response of polymeric materials to the creep-recovery test depends on the molecular structure and morphology (degree of crystallinity) of the material, magnitude, and duration of applied stress and temperature. The reason for some permanent and irreversible deformations on some polymers during creep and creep-recovery tests is due to the movement of molecular segments on the amorphous regions and reorientations on the crystalline regions.[26]

During the creep experiment, a constant stress ($\tau_o = 5$ Pa) was applied instantaneously ($t = 10$ s) to PIn/SO and PIn/O-MMT/SO suspensions, and changes in γ were measured over a period of time under $E = 0$ and $E = 2$ kV/mm conditions. Then the applied stress was removed ($\tau_o = 0$ Pa) and the time dependent deformations were recorded.

The creep and creep-recovery behavior of K2/SO system is depicted in Figure 12 under (a) $E = 0$ kV/mm and (b) $E = 2$ kV/mm conditions. It was observed that under $E = 0$ kV/mm condition, the γ increased rapidly and continiously with time under the applied stress of 5 Pa. After the applied stress was removed ($\tau = 0$ Pa), there was no instantenous elastic recovery, corresponding to a non-recoverable viscous deformation at the end of 10 s, which indicates that energy used for bond stretchings are not stored and totally distributed.[27] On the other hand, under $E = 2$ kV/mm, following changes were recorded at the creep phase: (i) instantenous elastic response (γ_s), (ii) retarded elastic deformation (γ_d), (iii) viscous flow (γ_v) as a result of linear increase in strain. Besides, at the recovery phase under $E = 2$ kV/mm, the following changes were observed: (i) recovery of instantenous strain (γ_e), (ii) unreversible viscoelastic recovery (γ_v).

In conclusion, non-linear viscoelastic behaviors were recorded for the materials under E, since $\gamma_s \neq \gamma_e$. The recoverable strain is a measure of elasticity of materials which is an indication of solid-like behavior of the suspensions under E. These results showed that PIn/O-MMT nanocomposites became polarized under E and stored the electric field induced deformation, thus classified as smart

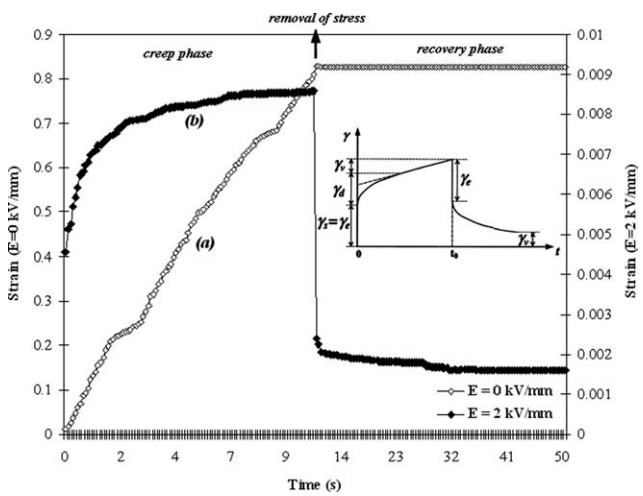

Figure 12 Creep and creep-recovery response of K2/SO suspension (a) $E = 0$ kV/mm, (b) $E = 2$ kV/mm (φ = 25%, $T = 25$°C).

materials. For the four materials examined in this work, percentage recoverable strain data are given in Table I, which is calculated from the following equation:

$$\text{recoverable strain } (\%) = \frac{\gamma_i - \gamma_f}{\gamma_i} \times 100 \qquad (4)$$

where γ_i is the total strain acquired before removing the applied stress and γ_f is the average steady state strain after removing the applied stress.[28]

As seen from Table I, viscoelastic recoveries were determined for all the materials examined under $E = 2$ kV/mm. As expected, percentage recoverable strains of the materials were increased with increasing PIn content of the nanocomposites and changed in the following order: PIn > K1 > K2 > K3, which may be attributed to the stronger structural orientation of the nanocomposites with increasing amount of PIn content.

CONCLUSIONS

Anti-sedimentation stabilities of the PIn/O-MMT/SO suspension systems were observed to suitable for potential industrial applications. ER activity of all the suspensions was observed to increase with increasing E, φ, and decreasing T and $\dot{\gamma}$; and showing a typical shear thinning non-Newtonian viscoelastic behavior. The high temperature conditions affected the storage modulus of the suspensions positively. Non-linear recoverable viscoelastic creep behavior was observed for all PIn/O-MMT nanocomposite/SO systems and recoverable strains were observed to decrease with increasing O-MMT content. Furthermore, 66% vibration damping capacity was determined for the Na-MMT/SO suspension system from the automobile shock absorber experiments under applied electric field strength, which is an important property from industrial point of view.

References

1. Tao, T. Adv Mater 2001, 13, 1847.
2. Wang, B.-X.; Zhao, X-P.; Zhao, Y.; Ding, C.-L. Compos Sci Technol 2007, 67, 3031.
3. Tao, T. Adv Colloid Interface 2002, 97, 1.
4. Espin, M. J.; Delgado, A. V.; Plocharski, J. Rheol Acta 2006, 45, 865.
5. Hao T. Stud Interface Sci 2005, 22, 114.
6. Fang, F. F.; Choi, H. J.; Joo, J. J Nanosci Nanotechnol 2008, 8, 1559.
7. Lu, J.; Zhao, X. J Mater Chem 2002, 12, 2603.
8. Cheng, Q.; Pavlinek, V.; Lengalova, A.; Li, C.; Belza, T.; Saha, P. Microporous Mesoporous Mater 2006, 94, 193.
9. Erol, O.; Unal, H. I.; Sari, B. Polym Compos 2010, 31, 471.
10. Guzel, S.; Unal, H. I.; Erol, O.; Sari, B. J Appl Polym Sci, to appear. DOI: 10.1002/app.34922.
11. Sarikaya, S. Yavuz, M. Yilmaz, H. Unal, H. I. Sari, B. Polym Compos 2009, 30, 583.
12. Lu, J.; Xiaopeng, Z. J Colloid Interface Sci 2004, 273, 651.
13. Espin, M. J.; Delgado, A. V.; Rejon, L. J Non-Newton Fluid 2005, 125, 1.
14. Shuizhu, W.; Jiarui, S. J Appl Polym Sci 1996, 60, 2159.
15. Klingenberg, D. J.; Zukoski, C. F. Langmuir 1990, 6, 15.
16. Xu, Y.; Liang, R. F. J Rheol 1991, 35, 1355.
17. Shuizhu, W.; Jiarui, S. J Appl Polym Sci 1996, 60, 2159.
18. Choi, U. S.; Ahn, B. G. Colloid Surf A 2000, 168, 71.
19. Choi, U. S.; Ko, Y. G.; Kim, J. Y. Polym J 2000, 32, 501.
20. Winslow, W. M. Field Response Force Transmitting Compositions. US Pat. 1962;30,47,507.
21. Conrad, H.; Chen, Y. Progress in Electrorheology; Plenum Press: New York, 1970, p 55.
22. Hao, T. Stud Interface Sci 2005, 22, 152.
23. Kim, S. G.; Lim, J. Y.; Sung, J. H.; Choi, H. J.; Yongsok, S. Polymer 2007, 48, 6622.
24. Hiamtup, P.; Sirivat, A.; Jamieson, A. M. J Colloid Interface Sci 2006, 295, 270.
25. Ergin, T. The Investigation of Efficiency and Vibration Damping Capabilities of Automotive Shock Absorbers; MSc thesis, Gazi University, Institute of Sciences: Ankara, 2006.
26. Genovese, A.; Shanks, R. A. Macromol Mater Eng 2007, 292, 184.
27. Li, W. H.; Du, H.; Chen, G.; Yeo, S. H. Mater Sci Eng A 2002, 333, 368.
28. Cho, M. S.; Lee, C. H.; Kim, J. W.; Suh, K. D. J Mater Sci 2004, 39, 1377.